Origin of the Repulsive Casimir Force in Giant Polarization-Interconversion Materials

Zhou Li [1,2,3,*] and Chinmay Khandekar[1]

[1]*Purdue University, West Lafayette, Indiana 47906, USA*

[2]*GBA Branch of Aerospace Information Research Institute, Chinese Academy of Sciences, Guangzhou 510535, China*

[3]*University of Chinese Academy of Sciences, Beijing 100039, China*

Achieving strong repulsive Casimir forces through engineered coatings can pave the way for micro- and nanoelectromechanical applications where adhesive forces currently cause reliability issues. Here, we exploit Lifshitz theory to identify the requirements for repulsive Casimir forces in gyrotropic media for two limiting cases (ultrastrong gyroelectric and nongyroelectric). We show that the origin of repulsive force in media with strong gyrotropy such as Weyl semimetals arises from the giant interconversion of polarization of vacuum fluctuations.

I. INTRODUCTION

The Casimir force [1–5] exists between charge-neutral bodies separated by submicrometer gaps because of the quantum fluctuations of electromagnetic fields. It competes with other forces in the micro-to-nanometer region. For the majority of geometric and material configurations, the Casimir force is known to be attractive. Realizing repulsive Casimir force is not only fundamentally useful but also technologically relevant for micro- and nanoelectrome- chanical systems (MEMS and NEMS). From an engineer- ing perspective, attractive Casimir force dominates in the submicrometer regime where closely spaced system parts tend to attract each other. Our findings of the repulsive Casimir force could be applied in the design of MEMS and NEMS, to avoid attraction-induced friction. Our find- ings of the mixed attractive-repulsive Casimir force could be applied to extract energy from vacuum fluctuations.

The most-studied geometry in the context of Casimir force [6–8] is that of two parallel plates of real, dis- persive materials separated by a vacuum gap, where the force is accurately described by Lifshitz theory based on the fluctuation-dissipation theorem [2,4]. One well- known approach to obtain repulsive Casimir force [9] is to use two plates of dielectric constants ϵ_1, ϵ_2 separated by a liquid medium of permittivity ϵ_l instead of vac- uum such that $\epsilon_1 < \epsilon_l < \epsilon_2$. Recent works have revealed other approaches such as the use of Teflon-coated metallic plates [10]. Another intriguing approach relies on exploit- ing topological materials to achieve repulsive Casimir

forces using topological materials. These include three- dimensional topological insulators and Weyl semimet- als [11–14], two-dimensional Chern insulators, and the graphene family [15–17]. However, the underlying mecha- nism, which gives rise to repulsive Casimir forces in these topological materials, has remained unexplored.

In this paper, we elucidate the origin of Casimir repul- sion between two ultrastrong gyrotropic plates [Eq. (3)]. Weyl semimetals are strong (not ultrastrong) gyrotropic medium, as illustrated in Fig. 1, the Casimir force has to be determined numerically. For the repulsive Casimir force, we choose the typical parameters of the dielectric tensor of a Weyl semimetal, which could be realized in machine- learning-assisted material growth. Strong gyrotropic media have recently opened up promising fundamental and tech- nological avenues for thermal radiation-based devices [18– 20] as well.

II. FORMALISM

We start from the Lifshitz theory of the Casimir free energy for two parallel plates separated by a vacuum gap, which is

$$\frac{E_c(d)}{A} = k_B T \times \sum_n \int \frac{d^2k}{(2\pi)^2} \text{Ln}[\det(1 - \mathbf{R_1}\mathbf{R_2}e^{-2k_1 d})], \tag{1}$$

where R_1 and R_2 are the reflection matrix for plate 1 and plate 2, $E_c(d)$ is the free energy, A is the area, k_1 is the absolute value of the imaginary part of the wave vector k_z, T is the temperature, and k_B is the Boltzmann constant. The sum over n is defined as $1/2(n = 0) + \sum_{n>0}$ with n
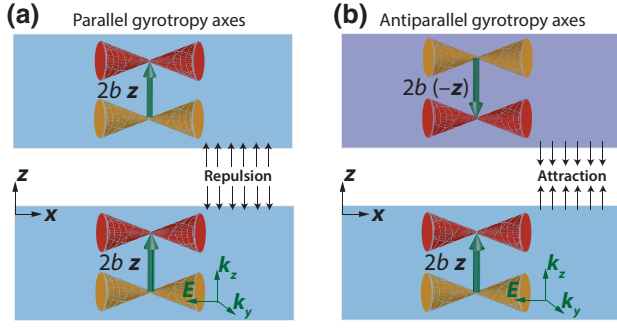
_____

*zli5@ualberta.ca

FIG. 1. Weyl semimetals are strong gyrotropic media whose gyrotropy axis is along the direction of the associated momentum-separation vector b of two Weyl nodes. (a) We show that for two plates with parallel gyrotropy axes, the Casimir force between the plates can become repulsive. (b) For plates with antiparallel gyrotropy axes, the Casimir force is always attractive.

the index of the Matsubara frequencies $\xi_n = 2\pi n k_B T/\hbar$. A reflection matrix for an electromagnetic wave injecting from one medium (e.g., the vacuum) to another medium (e.g., a silicon plate or gyrotropic plate) is defined as

$$\mathbf{R} = \begin{bmatrix} r_{ss} & r_{sp} \\ r_{ps} & r_{pp} \end{bmatrix},$$

where $r_{ss} = R_{\text{TE}}/A_{\text{TE}}$, $r_{sp} = R_{\text{TM}}/A_{\text{TE}}$, $r_{pp} = R_{\text{TM}}/A_{\text{TM}}$, and $r_{ps} = R_{\text{TE}}/A_{\text{TM}}$. Here $A_{\text{TM}}(R_{\text{TM}})$ are the amplitudes of injecting (reflected) TM mode, and $A_{\text{TE}}(R_{\text{TE}})$ are the amplitudes of injecting (reflected) TE mode. While the TE mode and the TM mode are orthogonal electromagnetic wave functions traveling in a vacuum, in other media, the electromagnetic eigenstates may be a mixture of TE and TM modes. Thus at the boundary of a vacuum and another medium, the TE mode to TM mode transfer ratio (r_{ps} and r_{sp}) could be nonzero. The Casimir force is the derivative of the Casimir energy, $F = -[\partial E_c(d)/\partial d]$. If $F > 0$, the force is repulsive, if $F < 0$, the force is attractive. The Casimir pressure is defined as

$$P = F/A = k_B T \times \sum_n \int \frac{d^2 k}{(2\pi)^2} \left[-\frac{\partial \text{Ln}(L)}{\partial d} \right], \quad (2)$$

where $L = \det[1 - \mathbf{R_1 R_2} e^{-2k_1 d}]$. While in general the repulsive Casimir force should be verified numerically, in two limit cases (ultrastrong gyrotropic and nongyrotropic), we provide here the requirement for a repulsive Casimir force in its basic form, with details given in the Appendix. For a ultrastrong gyrotropic material, the reflection coefficients $|r_{sp}|$ and $|r_{ps}|$ are much larger than $|r_{ss}|$ and $|r_{pp}|$, the requirement for a repulsive force is

$$\sum_n \int \frac{d^2 k}{(2\pi)^2} (r_{sp1} r_{ps2} + r_{ps1} r_{sp2}) < 0. \quad (3)$$

For a nongyrotropic isotropic medium, $r_{sp1} = r_{ps1} = 0$ and $r_{sp2} = r_{ps2} = 0$, the requirement for a repulsive force is

$$\sum_n \int \frac{d^2 k}{(2\pi)^2} (r_{ss1} r_{ss2} + r_{pp1} r_{pp2}) < 0. \quad (4)$$

This requirement also holds for the weak gyrotropic material where $|r_{sp}|$ and $|r_{ps}|$ are much smaller than $|r_{ss}|$ and $|r_{pp}|$.

Based on the Dirac-Maxwell correspondence, we define a Maxwell Hamiltonian and obtain the reflection coefficients ($r_{ss}, r_{pp}, r_{sp}, r_{ps}$) by connecting the wave functions (eigenstates) at the interface. The Maxwell equations for a specific medium (omitting the magnetoelectric media) is given by

$$\begin{bmatrix} \epsilon & 0 \\ 0 & \mu \end{bmatrix} \frac{\partial}{\partial t} \begin{bmatrix} \mathbf{E} \\ \mathbf{H} \end{bmatrix} = \begin{bmatrix} \nabla \times \mathbf{H} \\ -\nabla \times \mathbf{E} \end{bmatrix}, \quad (5)$$

where $\mathbf{E}$ and $\mathbf{H}$ are the electric and magnetic fields. Note that $(\mathbf{S} \cdot \nabla)\mathbf{H} = i\nabla \times \mathbf{H}$ where $\mathbf{S}$ is the spin-1 matrices with S_x, S_y, and S_z defined as,

$$S_x = \begin{bmatrix} 0 & 0 & 0 \\ 0 & 0 & -i \\ 0 & i & 0 \end{bmatrix}, \quad S_y = \begin{bmatrix} 0 & 0 & i \\ 0 & 0 & 0 \\ -i & 0 & 0 \end{bmatrix},$$

$$S_z = \begin{bmatrix} 0 & -i & 0 \\ i & 0 & 0 \\ 0 & 0 & 0 \end{bmatrix}.$$

Maxwell equations transform into a Dirac-like equation [21–23]. Assuming a plane wave $e^{i\mathbf{k} \cdot \mathbf{r} - i\omega t}$ of the electromagnetic field, we obtain the Maxwell Hamiltonian ($\omega = i\xi_n$)

$$H_{\text{Max}} = \begin{bmatrix} 0 & \epsilon^{-1}\mathbf{S} \cdot \mathbf{k} \\ -\mu^{-1}\mathbf{S} \cdot \mathbf{k} & 0 \end{bmatrix}. \quad (6)$$

For the Casimir force, the permittivity matrix at imaginary Matsubara frequencies $\omega = i\xi_n$ is relevant. With gyrotropy axis along the z direction, the permittivity matrix and its inverse are given below:

$$\epsilon = \begin{bmatrix} \epsilon_1 & g & 0 \\ -g & \epsilon_1 & 0 \\ 0 & 0 & \epsilon_2 \end{bmatrix}, \quad \epsilon^{-1} = \begin{bmatrix} d_1 & g' & 0 \\ -g' & d_1 & 0 \\ 0 & 0 & d_2 \end{bmatrix}. \quad (7)$$

Both are real valued at imaginary Matsubara frequencies. Here $d_1 = \epsilon_1/(\epsilon_1^2 + g^2)$, $d_2 = 1/\epsilon_2$ and $g' = -g/(\epsilon_1^2 + g^2)$. For a plane wave traveling in the $k_x - k_z$ plane, with

the wave vector $\mathbf{k} = (k_x, 0, q)$, the eigenvalue is given by

$$\xi_n^2 = -\left[(d_1 + d_2)k_x^2 + 2d_1 q^2 \mp \sqrt{P}\right]/2, \qquad (8)$$

here $P = k_x^4(d_1 - d_2)^2 - 4(k_x^2 + q^2)q^2 g'^2$ and we set $c = 1$, so ξ_n/c is written as ξ_n. We obtain an inverse solution of q from ξ_n and k_x, which is

$$
\begin{aligned}
q^2 &= 1/[2(d_1^2 + g'^2)] \\
&\times \left[-d_1[(d_1 + d_2)k_x^2 + 2\xi_n^2] - k_x^2 g'^2 \pm \sqrt{\triangle}\right], \quad (9)
\end{aligned}
$$

where

$$\triangle = [d_1(d_1 - d_2) + g'^2]^2 k_x^4 - 4g'^2 \xi_n^2(\xi_n^2 + d_2 k_x^2). \quad (10)$$

This gives four solutions (eigenstates) of electromagnetic waves inside a gyroelectric medium. However, along one specific direction, only two solutions are allowed. The two momenta q_1 and q_2 are chosen by the following rules: along the direction $+z$, the plane waves should decay at infinity. This requires the imaginary part $\mathrm{Im}(q) > 0$, but the real part is not restricted, $\mathrm{Re}(q) > 0$ or $\mathrm{Re}(q) < 0$; along the direction $-z$, it requires the imaginary part $\mathrm{Im}(q) < 0$, with no restriction on the real part. In both cases we have $q_1 = -q_2^*$. The eigenstate is a function of the momenta q_1 and q_2, $\psi_1 = [e_{x1}, e_{y1}, e_{z1}, h_{x1}, h_{y1}, h_{z1}]^T = [E_1, H_1]^T$ and $\psi_2 = [e_{x2}, e_{y2}, e_{z2}, h_{x2}, h_{y2}, h_{z2}]^T = [E_2, H_2]^T$, given by $E_{1,2} = E(q_{1,2})$ and $H_{1,2} = H(q_{1,2})$, with

$$E(q) = \left[E_x, -g'q\xi_n^2, -d_2 k_x(d_1 k_x^2 + d_1 q^2 + \xi_n^2)\right], \quad (11)$$

where $E_x = q[(d_1^2 + g'^2)(k_x^2 + q^2) + d_1\xi_n^2]$ and

$$H(q) = i\xi_n\left[-g'q^2, d_1 k_x^2 + d_1 q^2 + \xi_n^2, g'k_x q\right]. \quad (12)$$

The details of obtaining the reflection coefficients are given in the Appendix. For a nongyroeletric medium, $g' = 0$ and $d_1 = d_2$, we obtain $q = iq_I$ from Eq. (9) where $q_I^2 = k_x^2 + \xi_n^2/d_1 = \varepsilon(i\xi_n)\xi_n^2/c^2 + k_x^2$.

III. GYROELECTRIC MEDIUM AND THE MAGNETO-PLASMA MODEL

Now we consider a gyroelectric medium, which has nonzero off-diagonal elements in a permittivity matrix, typically given by the following magnetoplasma model:

$$
\begin{aligned}
\epsilon = \epsilon_b - &\frac{\omega_p^2}{(\omega + i\Gamma)^2 - \omega_c^2} \\
&\times \begin{bmatrix} 1 + i\dfrac{\Gamma}{\omega} & -i\dfrac{\omega_c}{\omega} & 0 \\[2mm] i\dfrac{\omega_c}{\omega} & 1 + i\dfrac{\Gamma}{\omega} & 0 \\[2mm] 0 & 0 & \dfrac{(\omega + i\Gamma)^2 - \omega_c^2}{\omega(\omega + i\Gamma)} \end{bmatrix}. \quad (13)
\end{aligned}
$$

Here ω_p is the plasma frequency, ω_c is the cyclotron frequency. Γ is the inverse lifetime of the charge carriers inside the medium, microscopically determined by the scattering process from impurities, phonons, or other sources. The background dielectric constant $\epsilon_b = \epsilon_\infty + \epsilon_{\mathrm{inter}} + \epsilon_{\mathrm{lattice}}$, where ϵ_∞ is the high-frequency limit, $\epsilon_{\mathrm{inter}}$ and $\epsilon_{\mathrm{lattice}}$ are contributions from interband transitions and lattice vibrations, respectively [18]. In the Matsubara frequency domain $\omega = i\xi_n$, the permittivity matrix [Eq. (7)] is described by diagonal coefficients $\epsilon_1 = \epsilon_b + \{\omega_p^2(1 + \Gamma/\xi_n)/[(\xi_n + \Gamma)^2 + \omega_c^2]\}$, $\epsilon_2 = \epsilon_b + [\omega_p^2/\xi_n(\xi_n + \Gamma)]$ and the off-diagonal coefficient $g = \{-\omega_p^2(\omega_c/\xi_n)/[(\xi_n + \Gamma)^2 + \omega_c^2]\}$.

IV. STRONG GYROELECTRIC MEDIUM AND THE WEYL SEMIMETAL

The constitutive relations for an ideal Weyl semimetal is given by [24,25]

$$D = \epsilon_w \mathbf{E} + \frac{ie^2}{4\pi^2\hbar\omega}(2\mathbf{b} \times \mathbf{E} - 2b_0\mathbf{B}), \quad (14)$$

where ϵ_w (ϵ in Figs. 3 and 4) is the diagonal part of the dielectric constant of the Weyl semimetal. The first term in the bracket comes from the anomalous Hall effect, and contributes to the off-diagonal part of the dielectric constant. The second term in the bracket comes from the chiral magnetic effect, for simplicity we set $b_0 = 0$. Here $\mathbf{b}$ is the momentum separation of the two Weyl nodes, and we choose $\mathbf{b} = bk_z$ to be along the z direction. The typical frequency $\omega_b = (e^2 b/2\pi^2\hbar\epsilon_0)$ is defined from the anamolous Hall effect, where ϵ_0 is the vacuum permittivity. For $b = 0.5$ Å^{-1}, we have $\omega_b = 6949$ THz. The microscopic theory of obtaining these parameters is provided in Refs. [26–33]. For the longitudinal optical conductivity, one finds that the optical conductivity increases linearly as a function of the frequency ω [30]. Similarly it increases sublinearly in topological insulators [29]. After dividing by ω, the dielectric constant ϵ_w should not change too much as a function of ω, therefore, in the Matsubara frequency domain, we choose $\epsilon_1 = \epsilon_2 \simeq 1$ (see discussions below Eq.

TABLE I. Off-diagonal permittivity (g) in comparison with diagonal permittivity ϵ_1 for magnetoplasma model and Weyl semimetal.

	g $(n = 1)$	g $(n = 2)$
Magnetoplasma model	$0.076 \ll \epsilon_1$	$0.0096 \ll \epsilon_1$
Weyl semimetal	$6.0778 \gtrsim \epsilon_1$	$3.039 \gtrsim \epsilon_1$

(11) in Ref. [14]), and the off-diagonal part of the permittivity matrix to be $g = (\omega_b/\xi_n)$. For $n = 0$, we add a tiny positive number to ξ_0 to avoid the divergence.

In Table I we show the absolute values of the gyrotropic coupling (off-diagonal permittivity) for the Matsubara frequencies corresponding to $n = 1, 2$ with the diagonal permittivity $\epsilon_1 \approx 1$ for both models. For the magnetoplasma model we use $\omega_p = 120$ THz and $\omega_c = 24$ THz and for the Weyl semimetal we use $\omega_b = 1000$ THz. The temperature is assumed to be $T = 200$ K.

V. NUMERICAL RESULTS

In Fig. 2, we show that gyrotropy, i.e., nonreciprocity is not a sufficient condition for repulsive Casimir force. We present numerical results of the Casimir force (pressure), between a silicon plate and a gyrotropic (magnetoplasma) plate, which is clearly attractive. The frequency-dependent dielectric constant of silicon is given by $\epsilon_{Si} = \epsilon_{(Si)\infty} + (\epsilon_{(Si)0} - \epsilon_{(Si)\infty})[\omega_0^2/(\xi_n^2 + \omega_0^2)] + \{\omega_p^2/[\xi_n(\xi_n + \Gamma)]\}$, where $\omega_0 = 6.6 \times 10^{15}$ Hz,

$\omega_p = 3.6151 \times 10^{14}$ Hz, $\Gamma = 7.868 \times 10^{13}$ Hz, $\epsilon_{(Si)\infty} = 1.035$, and $\epsilon_{(Si)0} = 11.87$. As ϵ_b moves toward 1, the attractive Casimir force is greatly suppressed. In comparison, the Casimir pressure between two perfect conducting plates is $P_C = -(\hbar c\pi^2/240d^4)$ as we derive in the Appendix. At $d = 0.2$ μm, $P_C = -0.8$ Pa.

In Fig. 3 we present numerical results of the Casimir force (pressure), between two Weyl-semimetal plates. Because of strong gyrotropy as evident from Table I, vacuum fluctuations in the gap between the plates experience strong polarization conversion. The associated reflection coefficients satisfy the condition given by Eq. (3) for a suitable range of in-plane wave vectors leading to repulsive Casimir force between the plates. For the case of parallel gyrotropy axes, we plot the Casimir force with three different parameter sets represented by black, red, and gray curves, respectively. As the distance d is changed, the Casimir force is tuned from repulsive to attractive, or always repulsive, or tuned from attractive to repulsive, respectively. For the case of antiparallel gyrotropy axes, the Casimir force is always attractive, as represented by the blue curve. For the black curve ($\epsilon = 1$ and $\omega_b = 3000$ THz), the Casimir force is tuned to be zero at $d_0 = 0.41$ μm (stable equilibrium); for the gray curve ($\epsilon = 1.1$ and $\omega_b = 1000$ THz), the zero-Casimir-force point $d_0 = 0.052$ μm is an unstable equilibrium.
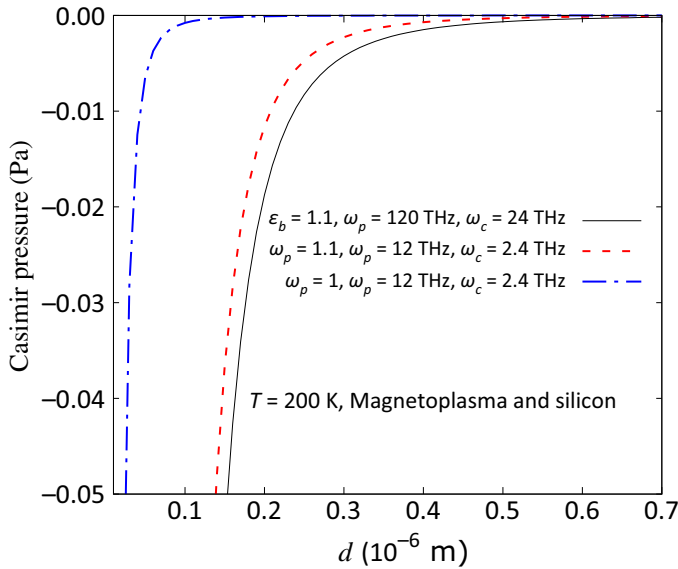

FIG. 2. Casimir pressure as a function of the distance, d, between a gyrotropic plate and a silicon plate. The dielectric constant of the gyrotropic plate is determined from the magnetoplasma model. Note that the Casimir force is always negative (attractive). When ϵ_b decreases from 1.1 to 1, the Casimir force is greatly suppressed.
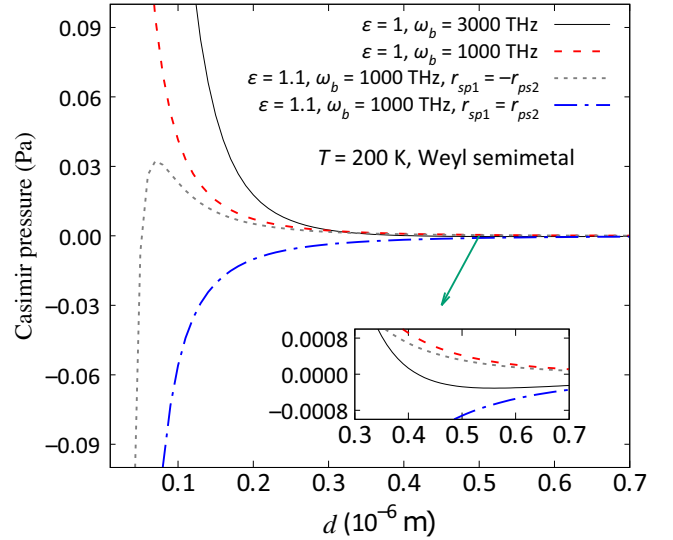

FIG. 3. Casimir pressure as a function of the distance, d, between two Weyl-semimetal plates. Note that for the blue dash-dotted curve, the two gyroaxis are antiparallel, we have $r_{sp1} = r_{ps2}$, and the Casimir force is always attractive. For the other three curves, the two gyroaxes are parallel, we have $r_{sp1} = -r_{ps2}$, the Casimir force is tuned from attractive to repulsive. The gray dotted curve crosses zero at around $d = 0.052$ μm (unstable equilibrium) and the black solid curve crosses zero at around $d = 0.41$ μm (stable equilibrium). For the red dashed curve, the Casimir force is always repulsive.
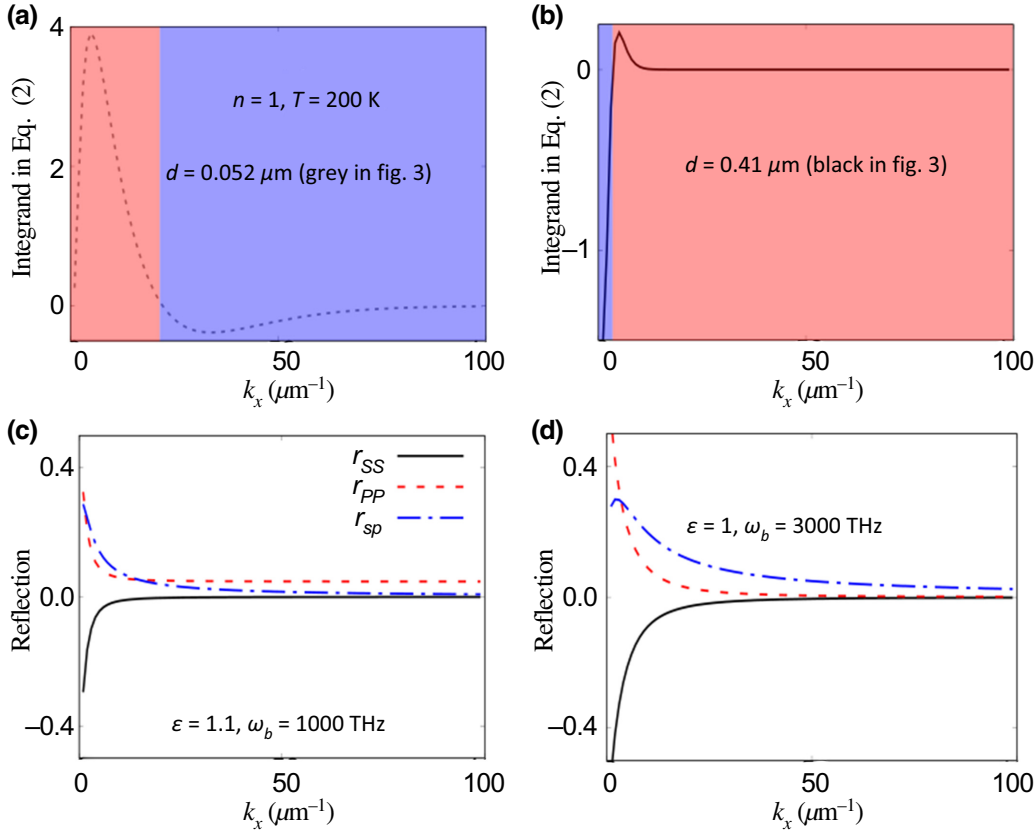
FIG. 4. The integrand $(k_x \times \{-[\partial \text{Ln}(L)/\partial d]\})$ in Eq. (2) [shown in (a),(b)] and the associated reflection coefficients [shown in (c),(d)] as a function of k_x. We set the Matsubara frequency at $n = 1$ and choose parameters the same as those of the black and gray curves in Fig. 3. We use the red (blue) color to denote the repulsive (attractive) contribution to the Casimir force, respectively, in (a),(b).

In Fig. 4 we investigate the origin of the stable and unstable equilibria, as shown in Fig. 3 by the black and gray curves, respectively. As Casimir forces depend on vacuum fluctuations at all momenta and frequencies, their interpretation is significantly more challenging than conventional narrowband (e.g., laser-driven) coherent optical forces. Therefore, we separately identify the contribution of specific plane waves to explain the origin of the repulsive Casimir force. We present the integrand of Eq. (2) in Fig. 4(b), as a function of k_x and fix the Matsubara frequency at $n = 1$. The black curve is negative (contribute to an attractive Casimir force) for small k_x and positive (contribute to a repulsive Casimir force) for large k_x. The gray curve shows an opposite trend. In Figs. 4(c) and 4(d) we plot the amplitude of the reflection coefficients for the gray curve and black curve, respectively. For Fig. 4(c), $|r_{sp}|$ is larger than $|r_{pp}|$ and $|r_{ss}|$ in a narrow range of k_x, while for Fig. 4(d) $|r_{sp}|$ is larger than $|r_{pp}|$ (or $|r_{ss}|$) in a broad range of k_x.

VI. CONCLUSION

In this paper we develop a theory of Casimir force based on the Lifshitz formula and the Dirac-Maxwell correspondence. We choose a magnetoplasma model and a Weyl semimetal model to apply the theory. We find repulsive Casimir force in the latter, which is a strong gyrotropic medium. We also find the repulsive Casimir force is tuned from repulsive to zero at specific distance (equilibrium). This could be applied in the design of MEMS (NEMS) to reduce the friction between tiny parts of devices.

APPENDIX A: DETAILS OF THE CONDITION FOR A REPULSIVE CASIMIR FORCE FROM THE REFLECTION MATRIX

Start from the Lifhtiz formula, the Casimir pressure is defined as

$$P = F/A = k_B T \times \sum_n \int \frac{d^2 k}{(2\pi)^2} \left[-\frac{\partial \text{Ln}(L)}{\partial d} \right], \quad \text{(A1)}$$

where

$$L = \det(1 - \mathbf{R_1}\mathbf{R_2}e^{-2k_1 d}), \quad \text{(A2)}$$

the product of the reflection matrices at interface 1 and 2 is given by

$$\mathbf{R_1 R_2} = \begin{bmatrix} r_{ss1} & r_{sp1} \\ r_{ps1} & r_{pp1} \end{bmatrix} \begin{bmatrix} r_{ss2} & r_{sp2} \\ r_{ps2} & r_{pp2} \end{bmatrix} = \begin{bmatrix} D_1 & D_2 \\ D_3 & D_4 \end{bmatrix},$$

where

$$D_1 = r_{ss1}r_{ss2} + r_{sp1}r_{ps2},$$
$$D_2 = r_{ss1}r_{sp2} + r_{sp1}r_{pp2},$$
$$D_3 = r_{ps1}r_{ss2} + r_{pp1}r_{ps2},$$
$$D_4 = r_{ps1}r_{sp2} + r_{pp1}r_{pp2},$$

with these definitions of D_1, D_2, D_3, and D_4,

$$L = 1 - (D_1 + D_4)e^{-2k_1 d} + (D_1 D_4 - D_2 D_3)e^{-4k_1 d}. \tag{A3}$$

The derivative of $\mathrm{Ln}(L)$, $-(\partial \mathrm{Ln}(L)/\partial d)$, is given by

$$\frac{-2k_1}{L}[(D_1 + D_4)e^{-2k_1 d} - 2(D_1 D_4 - D_2 D_3)e^{-4k_1 d}]. \tag{A4}$$

For a nongyrotropic case $r_{sp1} = r_{ps1} = 0$ and $r_{sp2} = r_{ps2} = 0$, so we have $D_1 = r_{ss1}r_{ss2}$, $D_4 = r_{pp1}r_{pp2}$, $D_2 = D_3 = 0$ and L is

$$1 - (r_{ss1}r_{ss2} + r_{pp1}r_{pp2})e^{-2k_1 d} + r_{ss1}r_{ss2}r_{pp1}r_{pp2}e^{-4k_1 d}. \tag{A5}$$

The derivative of $\mathrm{Ln}(L)$ becomes

$$-\frac{\partial \mathrm{Ln}(L)}{\partial d} = \frac{-2k_1}{L}[(D_1 + D_4)e^{-2k_1 d} - 2(D_1 D_4)e^{-4k_1 d}]. \tag{A6}$$

Then a repulsive force $F > 0$ requires the following:

$$\sum_n \int \frac{d^2 k}{(2\pi)^2} \frac{2k_1}{L} e^{-2k_1 d}[(D_1 + D_4) - 2D_1 D_4 e^{-2k_1 d}] < 0. \tag{A7}$$

Knowing that $k_1 > 0$, $L > 0$, and $e^{-2k_1 d} > 0$, we use an approximation that $(2k_1/L)e^{-2k_1 d}$ does not change too much in the sum of n and integral over k. The qualitative condition for a repulsive force is

$$\sum_n \int \frac{d^2 k}{(2\pi)^2}[(D_1 + D_4) - 2D_1 D_4 e^{-2k_1 d}] < 0. \tag{A8}$$

If the absolute value of the reflection coefficient satisfy the condition $|r_{ss}| < 1$ and $|r_{pp}| < 1$, known that $e^{-2k_1 d} < 1$, we have $|r_{ss1}r_{ss2}| > |r_{ss1}r_{ss2}r_{pp1}r_{pp2}|e^{-2k_1 d}$,

and $|r_{pp1}r_{pp2}| > |r_{ss1}r_{ss2}r_{pp1}r_{pp2}|e^{-2k_1 d}$, so $|D_1| + |D_4| > 2|D_1 D_4|e^{-2k_1 d}$, the dominant term is $D_1 + D_4$, the repulsive force condition simplifies as

$$\sum_n \int \frac{d^2 k}{(2\pi)^2}(r_{ss1}r_{ss2} + r_{pp1}r_{pp2}) < 0. \tag{A9}$$

For an ultrastrong gyrotropic material with giant polarization interconversion, we need to start from Eq. (A4). In this case, the reflection coefficients $|r_{sp}|$ and $|r_{ps}|$ could be much larger than $|r_{ss}|$ and $|r_{pp}|$, $D_1 \simeq r_{sp1}r_{ps2}$, $D_4 \simeq r_{ps1}r_{sp2}$, and $D_2 \simeq 0$, $D_3 \simeq 0$, follow the same logic we have

$$\sum_n \int \frac{d^2 k}{(2\pi)^2}(r_{sp1}r_{ps2} + r_{ps1}r_{sp2}) < 0. \tag{A10}$$

APPENDIX B: CASIMIR FORCE BETWEEN A PERFECTLY CONDUCTING PLATE AND AN INFINITELY PERMEABLE PLATE

For a perfectly conducting plate $\epsilon = \infty$ and $\mu = 1$, and for an infinitely permeable plate $\mu = \infty$ and $\epsilon = 1$. The reflection coefficients at the interface of a perfectly conducting plate and a vacuum is $r_{ss} = -1$ and $r_{pp} = 1$. The reflection coefficients at the interface of an infinitely permeable plate and a vacuum is $r_{ss} = 1$ and $r_{pp} = -1$. For both cases $r_{sp} = r_{ps} = 0$, so no polarization interconversion happens. At zero temperature, the sum of Matsubara frequencies becomes an integral $2\pi k_B T/\hbar \times \sum_n = \int d\xi$, assume the system is isotropic, so the integral over the angle θ gives 2π, the Casimir pressure is

$$P = \hbar/(2\pi) \int d\xi \int \frac{2\pi k dk}{(2\pi)^2} \left[-\frac{\partial \mathrm{Ln}(L)}{\partial d} \right]. \tag{B1}$$

We consider two cases below:

(i) Casimir force between two perfectly conducting plates,

$$L = 1 - 2e^{-2k_1 d} + e^{-4k_1 d}. \tag{B2}$$

The derivative of $\mathrm{Ln}(L)$ becomes,

$$-\frac{\partial \mathrm{Ln}(L)}{\partial d} = \frac{-2k_1}{L}[2e^{-2k_1 d} - 2e^{-4k_1 d}]. \tag{B3}$$

The attractive Casimir pressure is

$$P_C = -\frac{\hbar}{\pi^2} \int d\xi \int k_1 k dk \frac{e^{-2k_1 d}}{1 - e^{-2k_1 d}}. \tag{B4}$$

Knowing that $k_1^2 = k^2 + (\xi/c)^2$, we can introduce polar coordinates according to $k = k_1 \sin(\phi)$ and $\xi/c = k_1 \cos(\phi)$,

so $\int_0^\infty d(\xi/c) \int_0^\infty dk = \int_0^\infty k_1 dk_1 \int_0^{\pi/2} d\phi$, then the Casimir pressure is

$$P_C = -\frac{\hbar c}{\pi^2} \int_0^\infty k_1^3 dk_1 \int_0^{\pi/2} \sin(\phi) d\phi \frac{e^{-2k_1 d}}{1 - e^{-2k_1 d}}. \quad (B5)$$

Note that the integral

$$\int_0^\infty dx \frac{x^3 e^{-2x}}{1 - e^{-2x}} = \frac{\pi^4}{240}, \quad (B6)$$

we have

$$P_C = -\frac{\hbar c \pi^2}{240 d^4}. \quad (B7)$$

(ii) Casimir force between a perfectly conducting plate and an infinitely permeable plate,

$$L = 1 + 2e^{-2k_1 d} + e^{-4k_1 d}. \quad (B8)$$

The derivative of $\mathrm{Ln}(L)$ becomes

$$-\frac{\partial \mathrm{Ln}(L)}{\partial d} = \frac{-2k_1}{L}[-2e^{-2k_1 d} - 2e^{-4k_1 d}]. \quad (B9)$$

The repulsive Casimir pressure is

$$P_B = \frac{\hbar}{\pi^2} \int d\xi \int k_1 k dk \frac{e^{-2k_1 d}}{1 + e^{-2k_1 d}}. \quad (B10)$$

Follow the same logic in case (i) and note that the integral

$$\int_0^\infty dx \frac{x^3 e^{-2x}}{1 + e^{-2x}} = \frac{7\pi^4}{1920}, \quad (B11)$$

we have

$$P_B = \frac{7\hbar c \pi^2}{1920 d^4} = -(7/8)P_C. \quad (B12)$$

For a typical distance $d = 0.2\ \mu$m, $P_C = -0.8$ Pa.

APPENDIX C: REFLECTION MATRIX BETWEEN A VACUUM AND A GYROTROPIC PLATE

For more general cases with polarization interconversion, we solve the reflection coefficients in the way below. Assume the amplitudes of TM mode and TE mode are A_{TM} and A_{TE}, respectively, the injecting electromagnetic wave in the vacuum is

$$E_0 = (k_z A_{\mathrm{TM}}/\omega, A_{\mathrm{TE}}, -k_x A_{\mathrm{TM}}/\omega)e^{ik_x x + ik_z z - i\omega t} \quad \text{for } z > 0,$$

$$H_0 = (-k_z A_{\mathrm{TE}}/\omega, A_{\mathrm{TM}}, k_x A_{\mathrm{TE}}/\omega)e^{ik_x x + ik_z z - i\omega t} \quad \text{for } z > 0.$$

The reflected wave is

$$E_r = (-k_z R_{\mathrm{TM}}/\omega, R_{\mathrm{TE}}, -k_x R_{\mathrm{TM}}/\omega)e^{ik_x x - ik_z z - i\omega t} \quad \text{for } z > 0,$$

$$H_r = (k_z R_{\mathrm{TE}}/\omega, R_{\mathrm{TM}}, k_x R_{\mathrm{TE}}/\omega)e^{ik_x x - ik_z z - i\omega t} \quad \text{for } z > 0.$$

The transmitted wave inside a specific material is given by

$$E_t = (e_x, e_y, e_z)e^{ik_x x + iqz - i\omega t} \quad \text{for } z < 0,$$

$$H_t = (h_x, h_y, h_z)e^{ik_x x + iqz - i\omega t} \quad \text{for } z < 0.$$

To obtain the Fresnel coefficients for a gyrotropic slab, we first consider the injecting TE mode to be zero ($A_{\mathrm{TE}} = 0$) and write down the boundary conditions

$$
\begin{aligned}
(k_z/\omega)(A_{\mathrm{TM}} - R_{\mathrm{TM}}) &= A_1 e_{x1} + A_2 e_{x2}, \\
R_{\mathrm{TE}} &= A_1 e_{y1} + A_2 e_{y2}, \\
(k_z/\omega)(R_{\mathrm{TE}}) &= A_1 h_{x1} + A_2 h_{x2}, \\
(A_{\mathrm{TM}} + R_{\mathrm{TM}}) &= A_1 h_{y1} + A_2 h_{y2},
\end{aligned}
\quad (C1)
$$

from which we obtain the ratio of A_1 and A_2,

$$[(k_z/\omega)e_{y1} - h_{x1}]A_1 = A_2[h_{x2} - (k_z/\omega)e_{y2}], \quad (C2)$$

where $\psi_1 = [e_{x1}, e_{y1}, e_{z1}, h_{x1}, h_{y1}, h_{z1}]^T = [E_1, H_1]^T$ and $\psi_2 = [e_{x2}, e_{y2}, e_{z2}, h_{x2}, h_{y2}, h_{z2}]^T = [E_2, H_2]^T$ are the transmitted electromagnetic wave function inside a specific medium (gyrotropic or magnetoelectric), usually obtained numerically. We also obtain the following equations:

$$
\begin{aligned}
(k_z/\omega)(A_{\mathrm{TM}} + R_{\mathrm{TM}}) &= A_1(k_z/\omega)h_{y1} + A_2(k_z/\omega)h_{y2}, \\
2(k_z/\omega)(A_{\mathrm{TM}}) &= A_1[(k_z/\omega)h_{y1} + e_{x1}] \\
&\quad + A_2[(k_z/\omega)h_{y2} + e_{x2}], \\
2(k_z/\omega)(R_{\mathrm{TM}}) &= A_1[(k_z/\omega)h_{y1} - e_{x1}] \\
&\quad + A_2[(k_z/\omega)h_{y2} - e_{x2}],
\end{aligned}
\quad (C3)
$$

the Fresnel coefficients r_{pp} and r_{ps} are obtained,

$$
\begin{aligned}
r_{pp} &= R_{\mathrm{TM}}/A_{\mathrm{TM}} \\
&= \frac{A_1[(k_z/\omega)h_{y1} - e_{x1}] + A_2[(k_z/\omega)h_{y2} - e_{x2}]}{A_1[(k_z/\omega)h_{y1} + e_{x1}] + A_2[(k_z/\omega)h_{y2} + e_{x2}]},
\end{aligned}
\quad (C4)
$$

$$
\begin{aligned}
r_{ps} &= R_{\mathrm{TE}}/A_{\mathrm{TM}} \\
&= \frac{2(A_1 h_{x1} + A_2 h_{x2})}{A_1[(k_z/\omega)h_{y1} + e_{x1}] + A_2[(k_z/\omega)h_{y2} + e_{x2}]}.
\end{aligned}
\quad (C5)
$$

Then we consider the injecting TM mode to be zero ($A_{\mathrm{TM}} = 0$), the boundary conditions are given by

$$
\begin{aligned}
(k_z/\omega)(-R_{\mathrm{TM}}) &= C_1 e_{x1} + C_2 e_{x2}, \\
(A_{\mathrm{TE}} + R_{\mathrm{TE}}) &= C_1 e_{y1} + C_2 e_{y2}, \\
(k_z/\omega)(R_{\mathrm{TE}} - A_{\mathrm{TE}}) &= C_1 h_{x1} + C_2 h_{x2}, \\
(R_{\mathrm{TM}}) &= C_1 h_{y1} + C_2 h_{y2},
\end{aligned}
\quad (C6)
$$

from which we obtain the ratio of C_1 and C_2,

$$[(k_z/\omega)h_{y1} + e_{x1}]C_1 = -C_2[(k_z/\omega)h_{y2} + e_{x2}], \quad (C7)$$

and the following equations:

$$(k_z/\omega)(A_{TE} + R_{TE}) = C_1(k_z/\omega)e_{y1} + C_2(k_z/\omega)e_{y2},$$
$$2(k_z/\omega)(A_{TE}) = C_1[(k_z/\omega)e_{y1} - h_{x1}]$$
$$+ C_2[(k_z/\omega)e_{y2} - h_{x2}],$$
$$2(k_z/\omega)(R_{TE}) = C_1[(k_z/\omega)e_{y1} + h_{x1}]$$
$$+ C_2[(k_z/\omega)e_{y2} + h_{x2}], \quad (C8)$$

the Fresnel coefficients r_{ss} and r_{sp} are obtained,

$$r_{ss} = R_{TE}/A_{TE}c$$
$$= \frac{C_1[(k_z/\omega)e_{y1} + h_{x1}] + C_2[(k_z/\omega)e_{y2} + h_{x2}]}{C_1[(k_z/\omega)e_{y1} - h_{x1}] + C_2[(k_z/\omega)e_{y2} - h_{x2}]}, \quad (C9)$$
$$r_{sp} = R_{TM}/A_{TE}$$
$$= \frac{-2(C_1 e_{x1} + C_2 e_{x2})}{C_1[(k_z/\omega)e_{y1} - h_{x1}] + C_2[(k_z/\omega)e_{y2} - h_{x2}]}. \quad (C10)$$

---

[1] H. B. G. Casimir and D. Polder, The influence of retardation on the London-van der Waals forces, Phys. Rev. **73,** 360 (1948).

[2] G. M. Lifshitz, The theory of molecular attractive forces between solids, Sov. Phys. JETP **2,** 73 (1956).

[3] S. K. Lamoreaux, Casimir forces: Still surprising after 60 years, Phys. Today **60,** 40 (2007).

[4] G. L. Klimchitskaya, U. Mohideen, and V. M. Mostepanenko, The Casimir force between real materials: Experiment and theory, Rev. Mod. Phys. **81,** 1827 (2009).

[5] A. O. Sushkov, W. J. Kim, D. A. R. Dalvit, and S. K. Lamoreaux, Observation of the thermal Casimir force, Nat. Phys. **7,** 230 (2011).

[6] V. A. Yampol'skii, S. Savel'ev, Z. A. Mayselis, S. S. Apostolov, and F. Nori, Anomalous Temperature Dependence of the Casimir Force for Thin Metal Films, Phys. Rev. Lett. **101,** 096803 (2008).

[7] E. G. Galkina, B. A. Ivanov, S. Savel'ev, V. A. Yampol'skii, and F. Nori, Drastic change of the Casimir force at the metal-insulator transition, Phys. Rev. B **80,** 125119 (2009).

[8] V. A. Yampol'skii, S. Savel'ev, Z. A. Mayselis, S. S. Apostolov, and F. Nori, Temperature dependence of the Casimir force for bulk lossy media, Phys. Rev. A **82,** 032511 (2010).

[9] K. A. Milton, E. K. Abalo, P. Parashar, N. Pourtolami, I. Brevik, and S. A. Ellingsen, Repulsive Casimir and Casimir-Polder forces, J. Phys. A **45,** 4006 (2012).

[10] Rongkuo Zhao, Lin Li, Sui Yang, Wei Bao, Yang Xia, Paul Ashby, Yuan Wang, and Xiang Zhang, Stable Casimir equilibria and quantum trapping, Science **364,** 984 (2019).

[11] Adolfo G. Grushin and Alberto Cortijo, Tunable Casimir Repulsion with Three Dimensional Topological Insulators, Phys. Rev. Lett. **106,** 020403 (2011).

[12] Justin H. Wilson, Andrew A. Allocca, and Victor Galitski, Repulsive Casimir force between Weyl semimetals, Phys. Rev. B **91,** 235115 (2015).

[13] Qing-Dong Jiang and Frank Wilczek, Repulsive, enhanced, tunable, Phys. Rev. B **99,** 125403 (2019).

[14] M. Belén Farias, Alexander A. Zyuzin, and Thomas L. Schmidt, Casimir force between Weyl semimetals in a chiral medium, Phys. Rev. B **101,** 235446 (2020).

[15] W. K. Tse and A. H. MacDonald, Quantized Casimir Force, Phys. Rev. Lett. **109,** 236806 (2012).

[16] Pablo Rodriguez-Lopez and Adolfo G. Grushin, Repulsive Casimir Effect with Chern Insulators, Phys. Rev. Lett. **112,** 056804 (2014).

[17] Pablo Rodriguez-Lopez, Wilton J. M. Kort-Kamp, Diego A. R. Dalvit, and Lilia M. Woods, Casimir force phase transitions in the graphene family, Nat. Commun. **8,** 14699 (2017).

[18] Linxiao Zhu and Shanhui Fan, Persistent Directional Current at Equilibrium in Nonreciprocal Many-Body Near Field Electromagnetic Heat Transfer, Phys. Rev. Lett. **117,** 134303 (2016).

[19] Bo Zhao, Cheng Guo, Christina A. C. Garcia, Prineha Narang, and Shanhui Fan, Axion-field-enabled nonreciprocal thermal radiation in Weyl semimetals, Nano Lett. **20,** 1923 (2020).

[20] Chinmay Khandekar, Farhad Khosravi, Zhou Li, and Zubin Jacob, New spin-resolved thermal radiation laws for nonreciprocal bianisotropic media, New J. Phys. **22,** 123005 (2020).

[21] Konstantin Y. Bliokh, Daria Smirnova, and Franco Nori, Quantum spin Hall effect of light, Science **348,** 1448 (2015).

[22] T. V. Mechelen and Z. Jacob, Universal spin-momentum locking of evanescent waves, Optica **3,** 118 (2016).

[23] Farid Kalhor, Thomas Thundat, and Zubin Jacob, Universal spin-momentum locked optical forces, Appl. Phys. Lett. **108,** 061102 (2016).

[24] O. V. Kotov and Y. E. Lozovik, Giant tunable nonreciprocity of light in Weyl semimetals, Phys. Rev. B **98,** 195446 (2018).

[25] J.-R. Soh, F. de Juan, M. G. Vergniory, N. B. M. Schröter, M. C. Rahn, D. Y. Yan, J. Jiang, M. Bristow, P. Reiss, J. N. Blandy, Y. F. Guo, Y. G. Shi, T. K. Kim, A. McCollam, S. H. Simon, Y. Chen, A. I. Coldea, and A. T. Boothroyd, Ideal Weyl semimetal induced by magnetic exchange, Phys. Rev. B **100,** 201102(R) (2019).

[26] A. A. Burkov, Anomalous Hall Effect in Weyl Metals, Phys. Rev. Lett. **113,** 187202 (2014).

[27] A. Zyuzin and Rakesh P. Tiwari, Intrinsic anomalous Hall effect in type-II Weyl semimetals, JETP Lett. **103,** 717 (2016).

[28] Zhou Li and J. P. Carbotte, Longitudinal and spin-valley Hall optical conductivity in single layer MoS$_2$, Phys. Rev. B **86,** 205425 (2012).

[29] Zhou Li and J. P. Carbotte, Hexagonal warping on optical conductivity of surface states in topological insulator Bi$_2$Te$_3$, Phys. Rev. B **87,** 155416 (2013).

[30] Phillip E. C. Ashby and J. P. Carbotte, Magneto-optical conductivity of Weyl semimetals, Phys. Rev. B **87**, 245131 (2013).

[31] Phillip E. C. Ashby and J. P. Carbotte, Chiral anomaly and optical absorption in Weyl semimetals, Phys. Rev. B **89**, 245121 (2014).

[32] Ya. I. Rodionov, K. I. Kugel, and F. Nori, Effects of anisotropy and disorder on the conductivity of Weyl semimetals, Phys. Rev. B **92**, 195117 (2015).

[33] Ya. I. Rodionov, K. I. Kugel, B. A. Aronzon, and F. Nori, Effect of disorder on the transverse magnetoresistance of Weyl semimetals, Phys. Rev. B **102**, 205105 (2020).